

Predicting the Behaviour of Underground Openings in Rock

By
Nick Barton

SYNOPSIS

Rock masses range from intact homogeneous media, through regularly jointed assemblies of blocks, to heavily sheared and crushed clay-bearing fault zones. A brief review of the behaviour of openings created in these media, such as boreholes, tunnels and large mine openings, indicate some consistent trends. The fundamental failure mechanisms and requirements for support are believed to be strongly influenced in all cases by the volume changes accompanying potential failure. Failure, even in unjointed media, eventually occurs on failure surfaces such as extension fractures or shear fractures. A "plastic" zone may not strictly exist since the rock between the failure surfaces can be intact and relatively less highly stressed. Since the volume changes accompanying failure are to a great extent determined by the dilation (or contraction) along these failure surfaces or pre-existing discontinuities, an understanding of the latter is fundamental to the prediction of underground opening behaviour.

Careful measurements of model jointed media are used to demonstrate some of the volume changes that can be expected when rock masses are subjected to increased shear stress. The components of joint deformation such as closure and shear-induced dilation determine the type of response of individual rock masses. Attempts are made to provide a unifying description of rock mass shear strength based on discontinuum behaviour. Both the Q-system and the JRC/JCS index characterization of discontinuities are utilized here. The proposed criterion contrasts with the Hoek and Brown criterion, which primarily describes the strength of intact rock, with adjustments for jointed or crushed media.

Examples of discrete modelling of excavations in jointed media are given, using both physical and numerical models as examples. Particular attention is focused on the discrepancy between the behaviour of jointed media and the attempts to simulate these by means of continuum models. Tensile opening of joints and hysteresis on unloading due to shear are cited as reasons for the discrepancy. Examples of recent discrete element modelling using the UDEC method are described, to illustrate the prediction of the disturbed zone around tunnels.

KEY WORDS

Tunnels, boreholes, failure modes, shear strength, joints, dilation, scale effects, physical models, numerical modelling.

4th Manuel Rocha Memorial Lecture Lisbon, 12th October 1987

1. INTRODUCTION

There are three specialized disciplines of rock engineering that provide us with fascinating glimpses of the way rock behaves around underground openings. The three areas employ different specialists who do not often have the opportunity of communicating their different experiences to each other. Their employees have entirely different goals, yet their common interest is excavation stability in rock.

Table 1. Three categories of openings and their failure modes

Category	Rock characteristics	Failure modes*
1. Deep boreholes (Oil Industry)	Sedimentary rocks. Low intact strength. High Stress.	Shear failures, lamination buckling, «plastic» yielding
2. Deep mines (Mining Industry)	Massive, brittle rocks. High intact strength. High stress	Extension failures, rock bursting, slabbing, buckling
3. Shallow tunnels (Civil, Transport)	Jointed, altered rock, low mass strength, low stress levels	Extension, and shear failures on pre-existing discontinuities, rotational failures

* Failure mode descriptions deliberately simplified.

2. OBSERVED FAILURE MODES

(i) Deep Boreholes

Recent research efforts, funded mainly by international oil companies, have thrown light on the possible failure mechanisms around deep boreholes. The subject is far from closed. However it already appears likely that failure does not initiate at the borehole wall but somewhere inside the wall (Maury, 1987). Carefully instrumented experiments have also shown that the peak tangential stress levels occur well away from the wall (Bandis et al. 1987). Due to the disturbed and partly failed zone, the effective modulus of the rock is lower at the wall of the borehole than within the surrounding material.

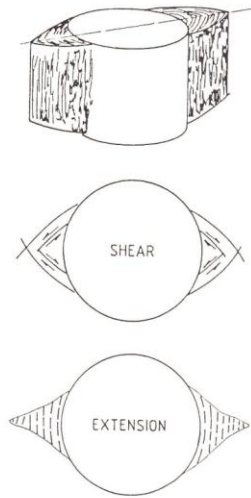


Fig. 1. Anisotropically loaded boreholes. Failure by shear and extension. Modified from Maury (1987). (Note that face advance effects on the failure mode are not represented in these two-dimensional simplifications.)

A dilemma remains concerning the mode of failure. This dilemma is illustrated in Fig. 1, which is extracted from Maury (1987) who was representing the ISRM Committee for Rock Failure Mechanisms in Underground Openings.

The concave-shaped elliptical overbreak typical for the shear failure mode contrasts with the convex-shaped overbreak and sharp "wedge" seen in the extension mode. Experience from borehole "dog-earing" in deep South African gold mines suggests the extension mode. Experience from physical models of boreholes in weak porous homogeneous materials proves without doubt that the shear mode is occurring.

Figures 2 and 3 illustrate some of NGI's experiences with boreholes drilled under three dimensional stress states in highly stressed, porous, brittle model materials. The curved shear failure surfaces resemble logarithmic spiral slip lines that have limited relationship to conventional "plastic" zones (Bandis et al. 1987). Furthermore, strength tests indicate that compaction and strain-hardening of material may occur during the successive redistribution of peak stress away from the borehole walls. Boreholes can be drilled and will remain more or less open under field stress levels several times larger than the unconfined compression strength of the materials concerned.

As a result of the above contrasts in behaviour between hard and soft rocks a tentative conclusion might be drawn. Strong brittle rocks under very high anisotropic stress can be expected to fail by successive deve-

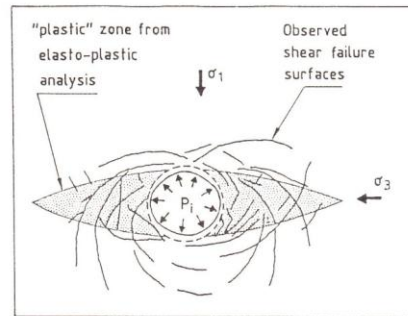


Fig. 2. Comparison of shear failure surfaces observed in a physical model, with the plastic zone predicted analytically. (Bandis and Nadim, 1985.)

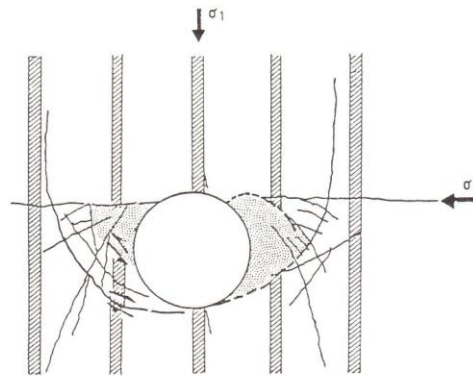


Fig. 3. Physical model simulation of boreholes drilled through highly stressed porous materials. (Bandis et al., 1987.) Line-drilled grouted holes provide markers and show shearing is the main failure mechanism.

lopment of extension fractures, while soft porous rocks under very high anisotropic stress can be expected to fail by the interaction of log-spiral-like shear surfaces. Possibly we can also go so far even at this stage, to suggest that the strong rock is still behaving in a dilatant failure mode, while the soft porous rock is behaving in a non-dilatant mode.

(ii) Deep Mines

A recent review of rock failure mechanisms in deep mines by Wagner (1987) supports in many respects the previous observations for boreholes. Massive brittle rocks (Fig. 4a) appear to fail in extension, and this mechanism is greatly accelerated if soft layers are present (Fig. 4c). Wedging or shear failure is seen in highly stressed coal measure rocks, which are softer and per-

haps non-dilatant at these high stress levels. Buckling and folding of thin strata is also a very common failure mechanism in such rocks.

A very interesting in situ experiment with a 1.5 m span tunnel in massive quartzites above an advancing stope face in a deep gold mine was described by Ortlepp and Gay (1984). Principal stress levels measured during tunnel driving are indicated in Figure 5. The tunnel was subsequently lightly supported with cable lacing and mesh and survived a final differential stress of almost 150 MPa during nearby reef mining. The sharp elliptical corners of the "failed" profile were apparently stable due to the rapid increase in confinement.

In massive "elastic" rock good use can apparently be made of the ratio of stress to strength when predicting onset of failure. The unconfined compression strength of laboratory-size samples can be compared with the principle stress (σ_1), with the vertical stress (σ_v), or with the maximum theoretical tangential stress ($3\sigma_1 - \sigma_3$ for a circular opening). However there are problems in this approach.

In the case of borehole size openings the unconfined strength of similar size rock specimens would appear relevant. However, as we have seen, the rock surrounding a deep borehole in weak reservoir-type environments does not behave elastically. It is therefore difficult to compare secondary stresses with strength. Paradoxically, in deep mining environments in massive rock where elastic theory might be more reliable, the size of

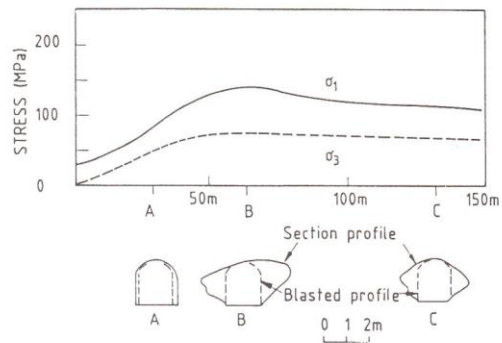


Fig. 5. Experimental tunnel in deep quartzites subjected to mining induced stress changes and partial failure. After Ortlepp and Gay (1984) and Wagner (1987).

excavation induces an important scale effect on the measured rock strength.

Hoek and Brown's (1980) empirical equation for the unconfined compression strength of 10 mm to 200 mm diameter laboratory specimens has been successfully extrapolated by South African workers (see Wagner, 1987) for application to fracturing in excavations in massive quartzites of 2 and 3 metres in span. Based on the data shown in Fig. 6 a logical simplification would be:

$$\sigma_c = \sigma_{c50} (50/d)^{0.2} \dots \dots \dots (1)$$

where σ_{c50} = unconfined compression strength of 50 mm specimens
 d = specimen diameter (mm)

This equation will later be compared with scaling rules used for extrapolating the shear strength of rock joints.

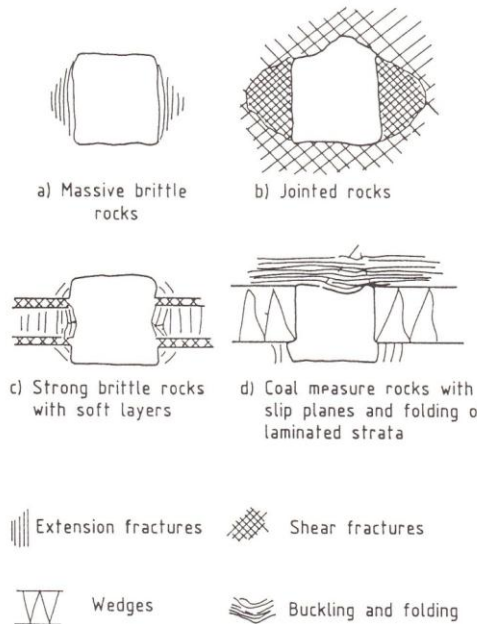


Fig. 4. Typical rock failures in highly stressed mine openings, after Wagner (1987).

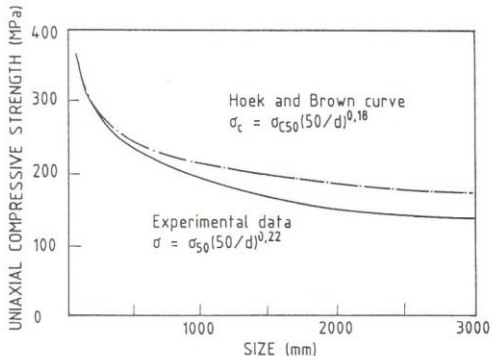


Fig. 6. Scale effects on unconfined compression strength. Comparison of extrapolated Hoek and Brown (1980) equation with South African mine failure data for quartzites. Wagner (1987).

(iii) *Shallow Tunnels*

In general shallow tunnels are driven in rock masses which are jointed, perhaps faulted, and often clay-bearing to a greater or lesser degree. The shallow tunnels may be road or rail tunnels, water supply or hydro power tunnels. Broadly speaking they can be called civil engineering tunnels. Obviously experiences within this category grade into the deep mining category, since similar problems of stress induced slabbing and even

rock bursting can be experienced in deep or anisotropically stressed road and hydro power tunnels.

Shallow tunnels in jointed rock masses may be unstable if they are driven through rock masses of low shear strength. The excavation span and the support used are obviously determining factors. In order to understand some of the important factors involved in failure of jointed rock masses it is instructive to examine some of the case records described by Cecil (1975) that formed the initial data base of the Q-system of rock mass classification (Barton et al., 1974).

The three cases illustrated in Fig. 7 show overbreak or local failure caused by clay-bearing shear zones or joints. The arrows indicating shear stress and shear resistance (added by this author) are designed to emphasize the role of shear strength in failure or stability. However, shear strength in the confined underground environment may be less important than the dilation occurring along the shearing surfaces prior to failure. It can be deduced that the presence of clay in the three cases shown in Fig. 7 may have allowed shear to occur without causing higher normal (tangential) stresses to develop. Overbreak or subsequent roof falls could therefore occur even if the joints actually shearing were dilatant.

The block sizes represented in the three cases in Fig. 7 suggest translational shear along the surfaces marked with arrows. Block rotations will only have occurred when partial failure (Stage "1") had already occurred, creating space for rotations. In contrast, the two heavily crushed rock masses illustrated in Fig. 8 had such small block sizes (relative to the scale of the problem) that rotational shearing was probably an admissible failure mode from the start, and of course would quickly become a rock "flow".

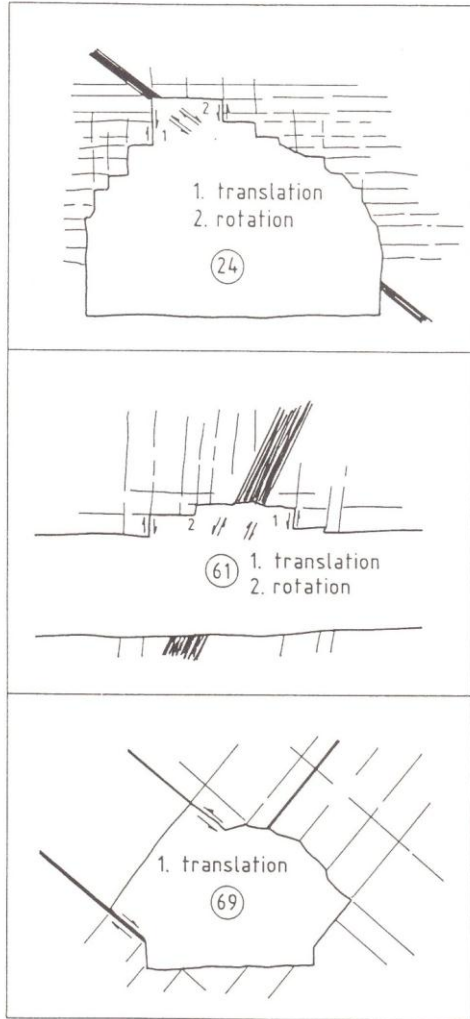


Fig. 7. Three examples of tunnel overbreak or partial failure, caused by translational shear along clay bearing discontinuities. (After Cecil, 1975.)

3. PRELIMINARY CONCLUSIONS ON FAILURE MODES

1. Deep boreholes in porous "non-elastic" rocks are likely to fail by shear surface development if the stress-strength ratio along these potential surfaces is such that shearing will be non-dilatant.
2. Deep boreholes and tunnels in strong "elastic" rocks are likely to fail by extension fracture development if the stress-strength ratio along potential shear surfaces is such that shearing would be dilatant. Since extension fracturing is also dilatant this mode will tend to be progressive, from the surface inwards, giving onion-skin-like features at the excavation boundaries. If shear fracture surfaces do develop it is likely that they will be minimal in number (two surfaces intersecting, or progressive) to minimise the incompatible dilation.
3. Tunnels in jointed, faulted rocks probably fail by translational shear if block sizes are large compared

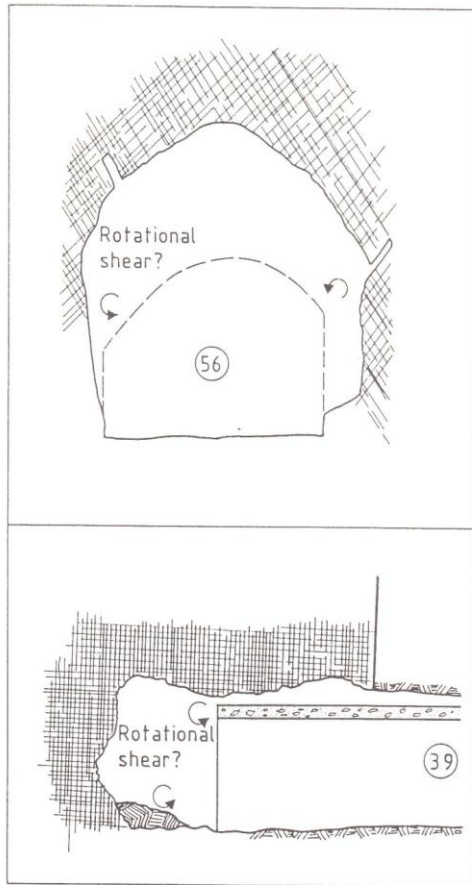


Fig. 8. Two examples of tunnel collapse caused by a clay bearing crushed zone in granite (case 56) and by a "sugar-cube" shear zone in quartzite (case 39). After Cecil, 1975.

to the tunnel dimensions. The small block sizes typical of crushed zones may allow rotational shear to occur as the primary mode since the required dilation is minimal, particularly if clay is present within the block structure.

- Formulations for the strength of rock masses that do not allow for the build-up of stress caused by dilatant failure, will predict larger fracture zones than observed in practice due to this limitation. This conservatism will be reflected in over designed tunnel reinforcement and support, a factor not present in empirical design methods due to the incorporation of observed behaviour which includes dilation, or contraction, as the case may be.

4. STRENGTH-DEFORMATION CHARACTERISTICS OF IDEAL ROCK MASSES

The importance of internal rock mass deformation, in particular dilation, on the behaviour of rock around tunnels has been established. How can we predict and quantify this characteristic for use in constitutive models?

Some clues to behaviour can be gained from an analysis of biaxial loading tests on jointed assemblies of blocks. Laboratory experiences with jointed physical models, and in situ block tests performed in current nuclear waste programmes provide us with some useful clues to behaviour.

(i) Physical models of idealized jointed rock

Figure 9 is a schematic illustration of a series of biaxial tests on jointed slabs of a brittle model material. In these models the first set of model joints (interlocking tension fractures) were continuous, while the second set were offset where crossing the pre-existing features. This is a realistic feature common to rock masses. The models were loaded by reduction of σ_2 and increase of σ_1 , giving the loading path shown in the upper diagram. The displacement vectors measured in one of the tests are reproduced in the lower diagram. The large lateral expansion (mass "Poisson's ratio") is apparent.

An analysis of the results of three such tests is shown in Fig. 10. Note that the lateral strain curves (marked ϵ_2) have been plotted on the same side of the y-axis as the axial stress-strain curves (marked ϵ_1), in order to save space. Of particular note are the rapidly increasing values of mass "Poisson's ratio" (ν) with increasing differential stress, and the radically different axial stress-strain curve of the model with 4000 interlocking blocks.

As block size was reduced, full scale moduli reduced from 18.5, to 13.1 and finally to 7.5 GPa. Nevertheless the highly jointed model exhibited the highest ultimate strength, and eventually failed by block rotation in the form of a broad kink band. The models with larger blocks failed by translational shear along a limited number of the most continuous joints.

The reasons for the higher strength with small block sizes is believed to be due to the extra freedom for block rotation given by deformable cross-joints. Small steep asperities therefore dominate behaviour, and the greater "mobility" of the smaller blocks eventually allows uncontrolled rotations to occur at ultimate strength.

The above biaxial stress-deformation data needs to be synthesised in dimensionless form so that it can be utilized in a constitutive model of rock mass behaviour. Relationships between the following may be useful:

$$\frac{(\sigma_1 - \sigma_2)}{2\sigma_c} \text{ versus } \nu \quad \text{or} \quad \frac{(\sigma_1 - \sigma_2)}{2 \cdot \tau_{\text{peak}}} \text{ versus } \nu$$

where

σ_c is the unconfined strength of individual rock blocks of known size, $(\sigma_1 - \sigma_2)/2$ is the shear stress level, τ_{peak} is the peak shear strength of the rock mass.

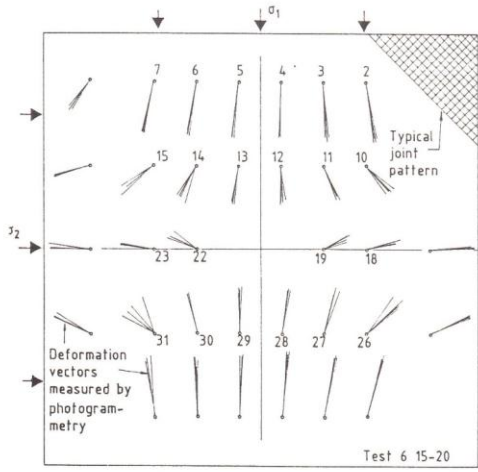
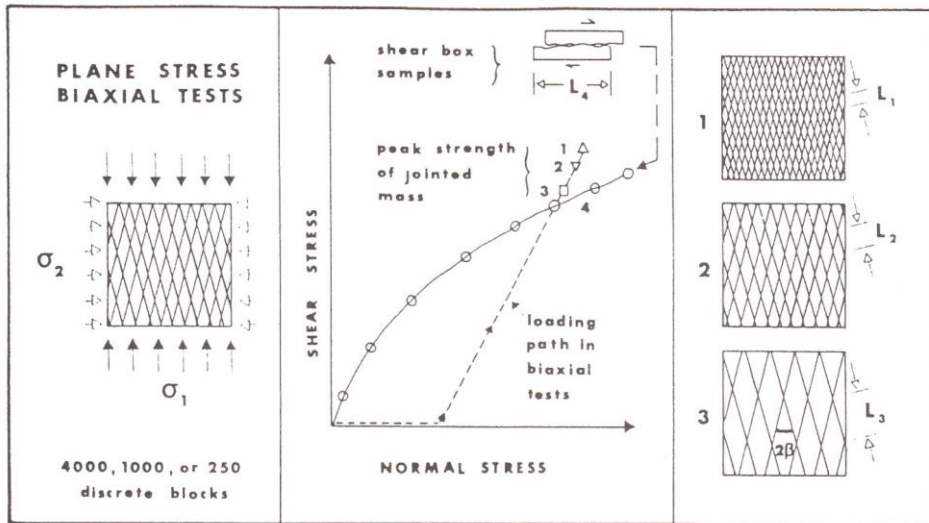


Fig. 9. Biaxial shear tests of idealized jointed rock masses indicate large lateral expansions; and block dependent ultimate strengths.

(ii) Joint deformation components in rock mass behaviour

The general shape of the stress-strain curves for rock masses can be deduced by considering the mechanics of joint deformation. In normal closure, joints exhibit strongly concave normal stress-deformation behaviour. In shear the stress-deformation behaviour is usually convex in shape, though this will depend on the block size.

Table 2. Tentative estimates of rock mass expansion characteristics as a function of differential stress level. (v = ratio of lateral/axial strain). Type R refers to cases with very small block sizes where rotational failure can occur.

$\frac{(\sigma_1 - \sigma_2)}{2\tau_{peak}}$	TYPE A*	TYPE B*	TYPE C*	TYPE R*
	v	v	v	v
0	0	0	0	0
0.2	0.2	0.25	0.30	0.1
0.4	0.2	0.35	0.45	0.1
0.6	0.4	0.55	0.7	0.2
0.8	0.5	0.7	1.0	0.3
1.0	>0.5	>0.75	>1.0	>0.4

* Type A, B, C refers to rock mass character (Figure 11).

The two components (N = normal, S = shear) shown in the upper diagrams in Fig. 11 combine to produce the three characteristic stress-strain curves for rock masses shown in the lower diagram of the same figure. Attempts have been made to incorporate some of the measured experiences from the model tests in the curves showing axial and lateral stress-strain.

In the following, an attempt will be made to propose dimensionless data relating the mass Poisson's ratio with the stress/strength ratio $(\sigma_1 - \sigma_2)/2\tau_{peak}$ for the three simple classes of rock mass represented in Fig. 10. The data is estimated or based on the model results depicted in Fig. 10. It is obviously extremely difficult to obtain such data for real rock masses due to the extremely high stresses required.

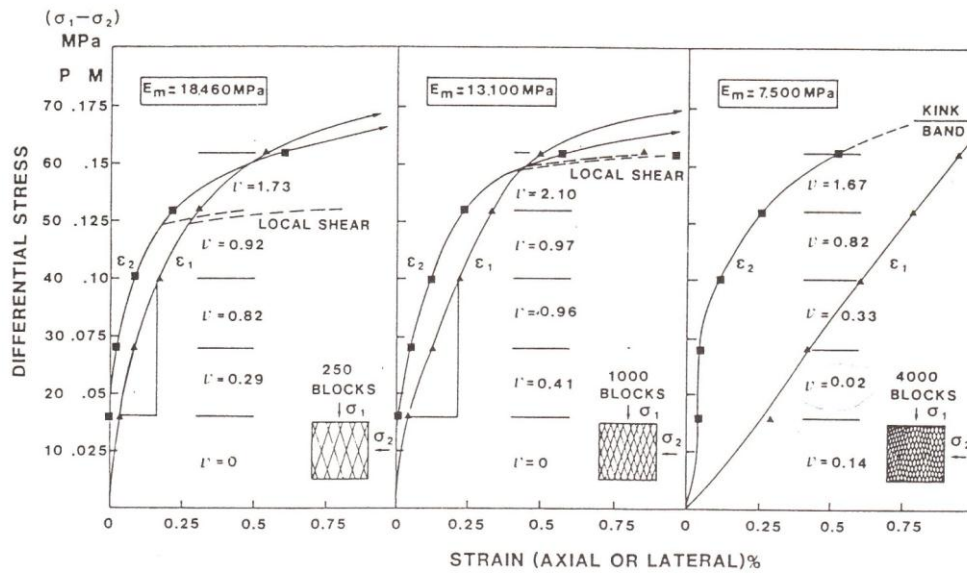


Fig. 10. Contrasting deformation behaviour exhibited by idealized rock masses consisting of different sized blocks. (Prototype unconfined compression strength of intact blocks = 175 MPa.)

Table 3. Estimate of apparent «shear strength» of rock masses from the parameters J_r and J_a used in the Q-system.

(a) Rock wall contact	J_r	$\tan^{-1} (J_r/J_a)^0$				
		$J_a = 0.75$	1.0	2	3	4
A. Discontinuous joints	4	79°	76°	63°	53°	45°
B. Rough, undulating	3	76°	72°	56°	45°	37°
C. Smooth, undulating	2	69°	63°	45°	34°	27°
D. Slickensided, undulating	1.5	63°	56°	37°	27°	21°
E. Rough, planar	1.5	63°	56°	37°	27°	21°
F. Smooth, planar	1.0	53°	45°	27°	18°	14°
G. Slickensided, planar	0.5	34°	27°	14°	9.5°	7.1°
(b) Rock wall contact when sheared	J_r	$\tan^{-1} (J_r/J_a)^0$				
		$J_a = 4$	6	8	12	
A. Discontinuous joints	4	45°	34°	27°	18°	
B. Rough, undulating	3	37°	27°	21°	14°	
C. Smooth, undulating	2	27°	18°	14°	9.5°	
D. Slickensided, undulating	1.5	21°	14°	11°	7.1°	
E. Rough, planar	1.5	21°	14°	11°	7.1°	
F. Smooth, planar	1.0	14°	9.5°	7.1°	4.7°	
G. Slickensided, planar	0.5	7°	4.7°	3.6°	2.4°	
(c) No rock wall contact when sheared	J_r	$\tan^{-1} (J_r/J_a)^0$				
		$J_a = 6$	8	12		
Disintegrated or crushed rock and clay	1.0	9.5°	7.1°	4.7°		
Bands of silty- or sandy-clay	1.0	$J_a = 5$				
		11°				
Thick continuous bands of clay	1.0	$J_a = 10$				
		5.7°	4.4°	2.9°		

5. SHEAR BEHAVIOUR OF INDIVIDUAL DISCONTINUITIES

The shear strength of individual joints or discontinuities obviously plays an important role in the shear resistance of the rock mass as a whole. A clear illustration of this fact is demonstrated by a Cundall et al. (1975) rigid block model of a "geologically" complex rock slope, reproduced in Fig. 12. In the more confined environment around a tunnel, the dilational characteristics of

the joints will have at least as much influence as the friction angle, due to the increase in normal stress that will accompany any tendency for shear.

(i) *Operating frictional angles deduced from Q-system parameters*

The Q-system of rock mass classification and tunnel support selection was developed after exhaustive trial and error with (eventually) six, parameters to describe

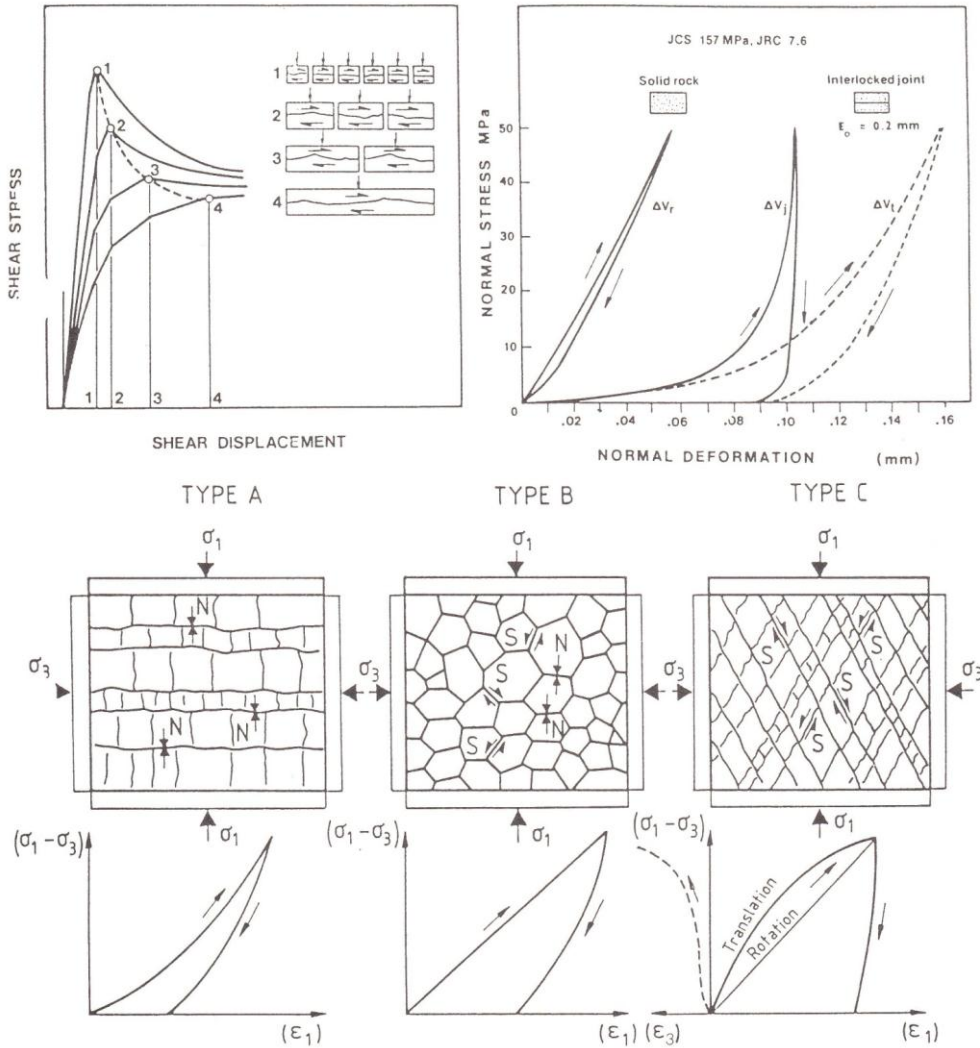


Fig. 11. Contrasting load-deformation behaviour for rock masses with different degrees of internal shear and normal deformation. Mass Poisson's ratio and hysteresis increase from Type A-B-C. Data for Type C derived from Fig. 10.

Table 4. Descriptions and ratings for the parameters J_r and J_a .

3. Joint Roughness number		4. Joint alteration number	
(a) Rock wall contact and (b) Rock wall contact before 10 cm shear		(J_a)	(ϕ_r) (approx.)
A. Discontinuous joints	4	A. Tightly healed, hard, non-softening, impermeable filling i.e. quartz or epidote	0.75 (-)
B. Rough or irregular, undulating	3	B. Unaltered joint walls, surface staining only	1.0 (25-35°)
C. Smooth, undulating	2	C. Slightly altered joint walls. Non-softening mineral coatings, sandy particles, clay-free disintegrated rock etc.	2.0 (25-30°)
D. Slickensided, undulating	1.5	D. Silty, or sandy-clay coatings, small clay fraction (non-soft.)	3.0 (20-25°)
E. Rough or irregular, planar	1.0	E. Softening or low friction clay mineral coatings, i.e. kaolinite or mica. Also chlorite, talc, gypsum, graphite etc., and small quantities of swelling clays	4.0 (8-16°)
F. Smooth, planar	0.5	(b) Rock wall contact before 10 cms shear	
Note: (i) Descriptions refer to small scale features and intermediate scale features, in that order.		F. Sandy particles, clay-free disintegrated rock etc.	4.0 (25-30°)
(c) No rock wall contact when sheared		G. Strongly over-consolidated non-softening clay mineral fillings (continuous, but <5 mm thickness)	6.0 (16-24°)
H. Zone containing clay minerals thick enough to prevent rock wall contact	1.0	H. Medium or low over-consolidation, softening, clay mineral fillings. (continuous but <5 mm thickness)	8.0 (12-16°)
J. Sandy, gravelly or crushed zone thick enough to prevent rock wall contact	1.0	J. Swelling -clay fillings, i.e. montmorillonite (continuous, but <5 mm thickness). Value of J_a depends on percent of swelling clay-size particles, and access to water etc.	8-12 (6-12°)
Note (ii) Add 1.0 if the mean spacing of the relevant joint set is greater than 3m.		(c) No rock wall contact when sheared	
Note (iii) $J_r = 0.5$ can be used for planar slickensided joints having lineations, provided the lineations are orientated for minimum strength.		K, L. Zones or bands of disintegrated or crushed rock and clay (see G, H, J for description of clay condition)	6, 8 or 8-12 (6-24°)
		N. Zones or bands of silty- or sandy-clay, small clay fraction (non-softening)	5.0 (-)
		O, P, R. Thick continuous zones or bands of clay (see G, H, J for description of clay condition)	10, 13, or 13-20 (6-24°)

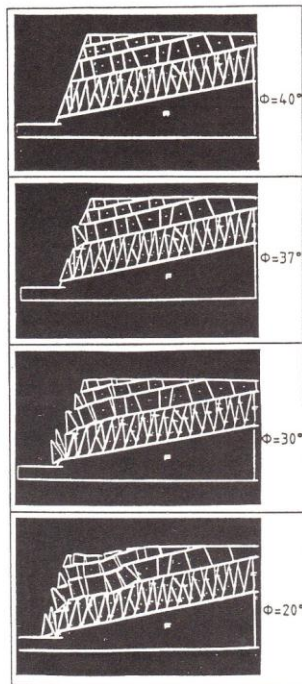


Fig. 12. A rigid block model of a rock slope illustrating the influence of joint friction angles on the failure mode. After Cundall et al. (1975).

rock mass characteristics (Barton et al., 1974). The individual ratings of the six parameters were successively adjusted in order to get the best fit between observed behaviour (i.e. the need for rock reinforcement) and the predicted reinforcement needs.

The six Q-system parameters have the following general form

1. RQD/J_n = equivalent block size
2. J_r/J_a = inter-block shear resistance
3. J_w/RSF = active stress

The "inter-block shear resistance" (J_r/J_a) resembles a limit equilibrium, back analysis result since, as shown in Table 3, the arctangent ($\tan^{-1} J_r/J_a$) happens to provide very realistic values of effective shear resistance, expressed as "friction angles". Table 4 should be refer-

red to for descriptions of the joint alteration and clay filling characteristics (J_a).

This "friction angle" finding is remarkable, since the extra significance of the ratio (J_r/J_a) was discovered by accident after the Q-system was developed. Of particular interest is the fact that both J_r (joint roughness number) and J_a (joint alteration number) are designed to apply to the "joint set or discontinuity most likely to initiate tunnel failure". In this respect $\tan^{-1}(J_r/J_a)$ resembles a limit equilibrium back-analysis result.

In the light of the foregoing discussion of the relative importance of friction angles and dilation characteristics, it is significant that Table 3 shows exaggeratedly high "friction angles" for the rough unweathered

joints which dilate most under shear (i.e. $\tan^{-1} J_r/J_a > 70^\circ$), and exaggeratedly low "friction angles" for the thick, clayfilled discontinuities which dilate least or even contract under shear (i.e. $\tan^{-1} J_r/J_a < 10^\circ$). Intermediate categories which dilate only slightly and at least do not contract under shear show values of $\tan^{-1}(J_r/J_a)$ which closely resemble friction angles measured in shear box tests under moderate normal stress levels, for example 1 MPa.

(ii) Prediction of the friction and dilation components of rock joints

A great deal of work has been performed on the shear strength of rock joints. As a result of many contributions, particularly those reviewed by Bandis (1980) and by Barton and Bahktar (1983) it is now possible to make quite accurate predictions of the peak shear strength, and of the shear strength-displacement and the displacement-dilation characteristics of rock joints over a wide range of block sizes. An example of this predictive capability is illustrated in Fig. 13.

The basic equations describing the friction angle (φ_m) and the dilation angle (d_m) mobilized at any given shear displacement, are based on the concept of mobilized roughness (JRC_m) which is defined in Fig. 14.

$$\varphi_m = JRC_m \log \left(\frac{JCS}{\sigma_n} \right) + \varphi_r \dots \dots \dots (2)$$

$$d_m = \frac{1}{2} JRC_m \log \left(\frac{JCS}{\sigma_n} \right) \dots \dots \dots (3)$$

where JCS = joint wall compression strength
 JRC = joint roughness coefficient
 φ_r = residual friction angle
 σ_n = effective normal stress

Evaluation of these two equations using the desired input data for JCS, JRC and φ_r and the simple table of dimensionless numbers given in Fig. 14, provides the necessary data for producing the laboratory scale shear stress-displacement and dilation-displacement curves shown in the example in Fig. 13. One additional equation is required however. This provides an estimate of the displacement (δ_{peak}) needed to reach peak shear strength.

$$\delta_{peak} = \frac{L_n}{500} \left(\frac{JRC_n}{L_n} \right)^{0.33} \dots \dots \dots (4)$$

where L_n = sample size, or in situ block size (spacing between cross-joints) in metres
 JRC_n = joint roughness coefficient of joints of length L_n

Example:
 $L_n = 1.0 \text{ m}$, $JRC_n = 5$
 equation 4 gives $\delta(\text{peak}) = 0.0034 \text{ m}$ (3.4 mm)

The need to consider block dimensions in this equation will be clear from the contrasting curves in Fig. 13. The table inset in the figure also indicates the scale effects acting on JRC and JCS.

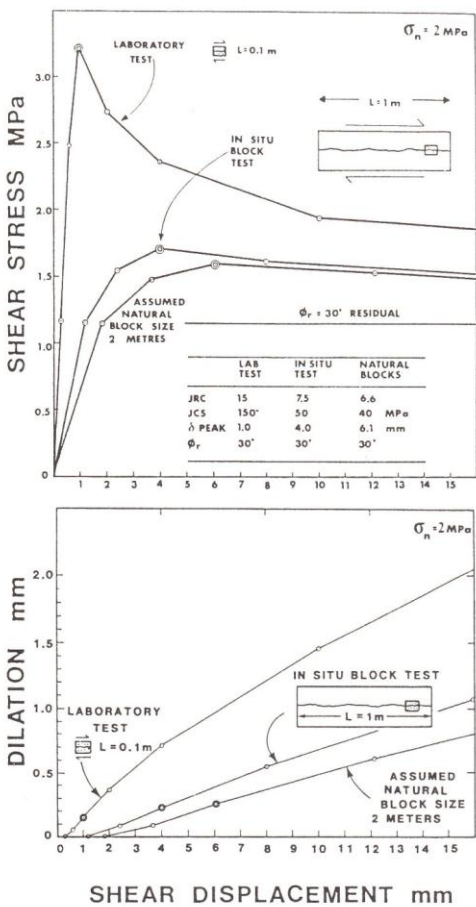


Fig. 13. Modelling the size-dependent shear stress-displacement and dilation-displacement behaviour of rock joints, assuming a constant effective normal stress of 2 MPa.

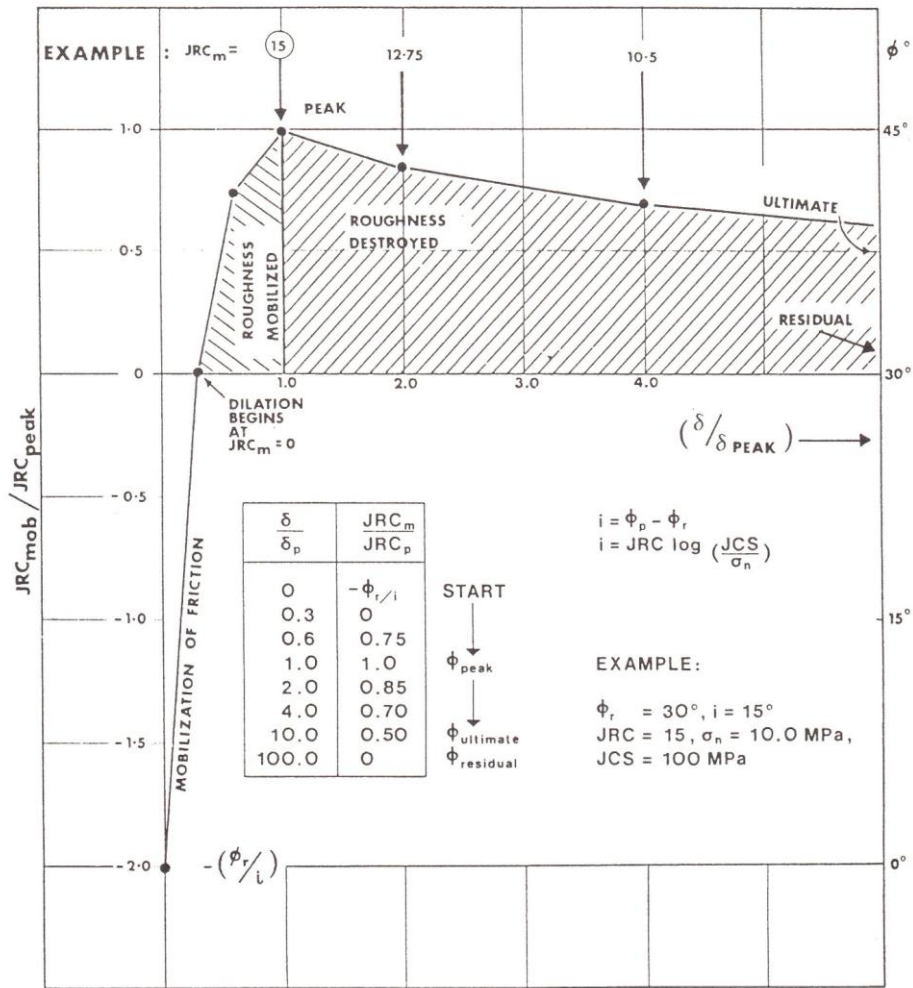


Fig. 14. The concept of roughness mobilization with increased shear displacement. In this example $JRC = 15$ represents the peak value of roughness.

(iii) Scale effects on asperity strength and surface roughness

Scale effects on JRC and JCS have been investigated by several authors (e.g. Barton and Choubey 1977, Bandis 1980). As a result of many experimental results Barton and Bandis (1982) produced the scale reduction factors shown in Fig. 15. Subscripts (o) and (n) refer to laboratory and in situ block sizes respectively.

Similar scale effects trends were exhibited in Fig. 6. This showed the scale effects on unconfined compression strength deduced by Hoek and Brown (1980), and those experienced in practice in South African tunnel failures (Wagner, 1987). The changing size of "signifi-

cant" asperities along a joint, as sample or block size increases, show similar trends of reduced strength to the scaling of unconfined compression strength. Constitutive equations of the trends exhibited in Fig. 15 are given below, and compare closely with the general form of equation 1.

$$JRC_n = JRC_o \left(\frac{L_n}{L_o} \right)^{-0.02 JRC_o} \dots \dots \dots (5)$$

$$JCS_n = JCS_o \left(\frac{L_n}{L_o} \right)^{-0.03 JRC_o} \dots \dots \dots (6)$$

Examples of the magnitude of these scale effects are given in the inset in Fig. 13.

(iv) Relationship between the J_r and JRC roughness descriptions

The descriptions of roughness given in the Q-system by the parameter J_r (see Table 4), and the more sophisticated parameter JRC just described, are obviously related. Fig. 16 has been prepared for the benefit of potential users of these rock mass descriptions. The ISRM (1978) suggested methods for visual description of joint roughness profiles have been combined with profiles given by Barton et al. (1980), and with the scaling equation 5, to produce some examples of the quantitative description of joint roughness that these parameters provide.

The roughness profiles drawn in Fig. 16 are assumed to be at least 1 metre in length. The column of J_r values would be used in the Q system, while the JRC_n values for 20 cm and 100 cm block sizes could be used to generate appropriate shear stress-displacement and dilation-displacement curves, such as illustrated in Fig. 13.

Relation between J_r and JRC_n Subscripts refer to block size (cm)		J_r	JRC_{20}	JRC_{100}
I	rough	4	20	11
	smooth			
	slickensided			
Stepped				
II	rough	3	14	9
	smooth			
	slickensided			
Undulating				
III	rough	1.5	7	6
	smooth			
	slickensided			
Planar				
IV	rough	1.5	2.5	2.3
	smooth			
	slickensided			
V	rough	1.0	1.5	0.9
	smooth			
	slickensided			
VI	rough	0.5	0.5	0.6
	smooth			
	slickensided			

Fig. 16. Suggested methods for the quantitative description of different classes of joints using the J_r and JRC_n concepts. Subscripts refer to block size (cm). The profiles are at least 100 cm in length.

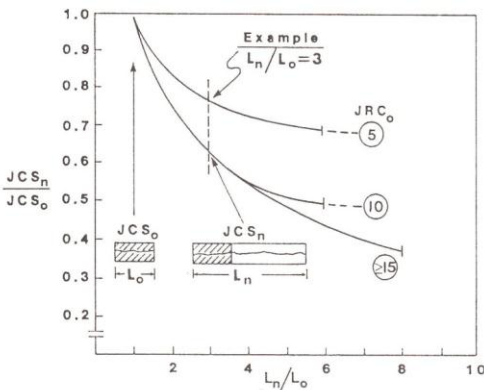
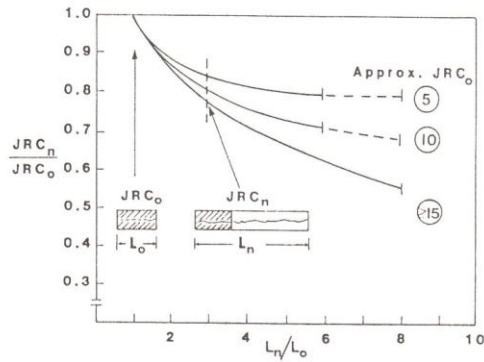


Fig. 15. Methods of scaling laboratory size values of JRC_o and JCS_o up to the full scale values (JRC_n , JCS_n) relevant for in situ block sizes L_n .

6. APPROXIMATE ESTIMATES OF THE SHEAR STRENGTH OF ROCK MASSES FOR TUNNEL STABILITY ANALYSES

(i) Hoek and Brown criterion

Hoek and Brown (1980) have produced an excellent treatise on the design problems encountered in underground excavation engineering. They have symbolized the problems involved in a useful figure which will be reproduced here (Fig. 17). Their illustration of the changing character of the rock mass with increasing scale can also be utilized to represent the wide range of rock qualities that can be encountered. One could for example suggest that the five sub-diagrams in Fig. 17 represent Q values of the order of 500, 100, 50, 10 and 1, if the five "samples" were of about the same dimensions as the underground excavation.

Hoek and Brown (1980) have listed several requirements for a rock failure criterion for use by underground excavation designers.

- "It should adequately describe the response of an intact rock sample to the full range of stress conditions likely to be encountered underground. These conditions range from uniaxial tensile stress to triaxial compressive stress."
- "It should be capable of predicting the influence of one or more sets of discontinuities upon the behavi-

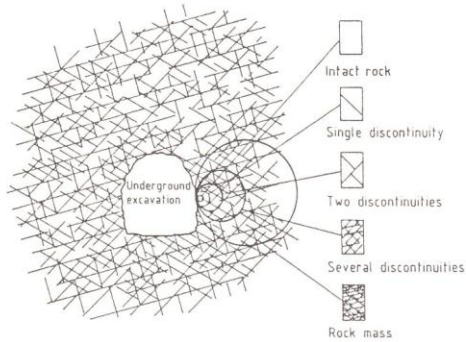


Fig. 17. The transition from intact rock to a heavily jointed rock mass with increasing sample size (Hoek and Brown, 1980).

our of a rock sample. This behaviour may be highly anisotropic, i.e. it will depend upon the inclination of the discontinuities to the applied stress direction.”

- c. “It should provide some form of projection, even if approximate, for the behaviour of a full scale rock mass containing several sets of discontinuities?”

The approach they finally adopted was to develop a new criterion describing the strength of intact rock and modify it directly, to account for the discontinuous nature of rock masses. Their basic equation was as follows:

$$\sigma_1 = \sigma_3 + \sqrt{m\sigma_c \sigma_3 + s\sigma_c^2} \dots \dots \dots (7)$$

where σ_1 = major principal stress at failure
 σ_3 = minor principal stress
 σ_c = unconfined compression strength of the intact rock

m and s are constants

The constant s = 1.0 for intact rock and reduces to 0 as the fracturing of the specimen (or degree of pre-existing jointing) increases. The constant (m) describes the curvature of the strength envelope and reflects the degree of particle interlock. As Hoek and Brown freely admit, the choice of (m) and (s) is extremely difficult for the case of rock masses. They utilize the RMR and Q system classification methods to help in this choice.

In essence Hoek and Brown (1980) utilize a criterion for the intact strength of the rock pieces, and attempt to modify it to account for the jointing. This philosophy contrasts with the approach which will be adopted here, which relies on established empirical equations for the shear strength of jointed and crushed rock.

(ii) A discontinuum-based strength criterion for rock joints and crushed rock

Barton and Kjærnsli (1981) showed that the peak friction angles (ϕ) of rock joints and crushed rock (i.e. rock fill) could be described by essentially the same equations:

1. rock joints $\phi_j = JRC \log (JCS/\sigma_n) + \phi_r \dots (8)$

2. crushed rock $\phi_c = R \log (S/\sigma_n) + \phi_b \dots \dots \dots (9)$

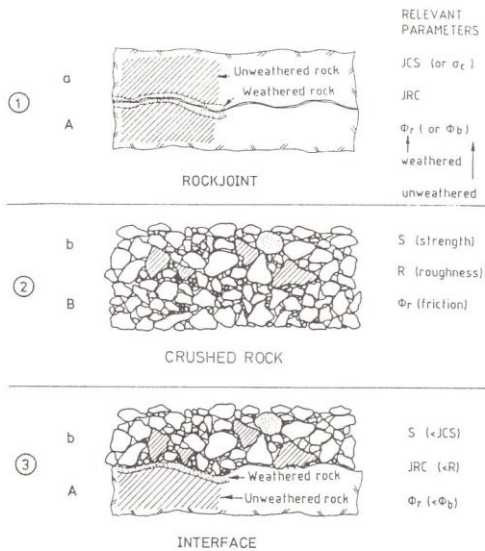


Fig. 18. Method of selecting input parameters for use in equations 8 and 9. (After Barton and Kjærnsli, 1981.)

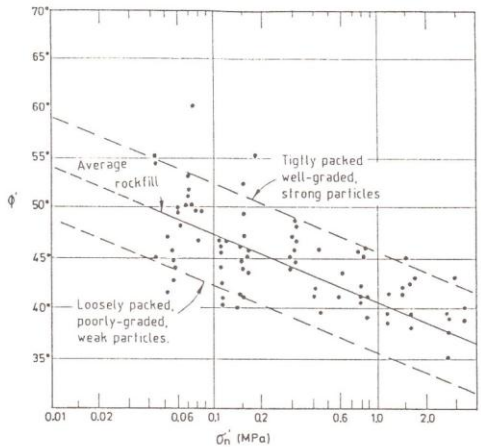


Fig. 19. Peak drained, friction angles for rock fill (Leps, 1970). Natural, crushed rock might correspond to the upper half of the data, i.e. average to tightly packed, but with adjustments for strength reductions due to hydrothermal alteration or weathering.

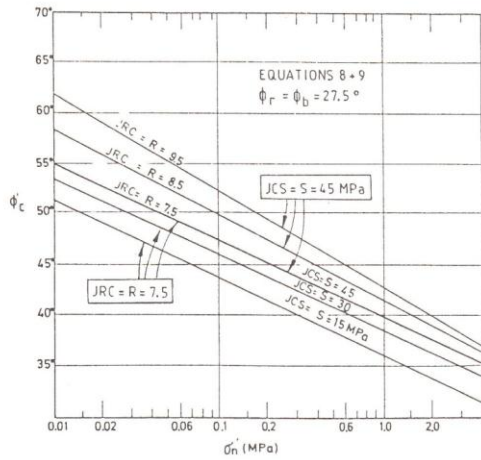


Fig. 20. Illustrations of the non-linearity of equations 8 and 9 describing the shear strength of rock joints and crushed rock (S, R and ϕ_b refer to crushed rock, JCS, JRC and ϕ_r refer to rock joints). Compare with Figure 19 test data.

where JRC, JCS and ϕ_r are as defined previously and $R =$ equivalent particle roughness, $S =$ equivalent particle strength.

Figure 18 illustrates how the choice of parameters JRC, JCS, R, S, ϕ_r and ϕ_b depends on the physical situation, i.e. whether the rock is jointed, crushed, or is an interface between the two. Simple index tests (tilt tests and Schmidt hammer tests) can be used to obtain the required input data, with suitable corrections for block size (Fig. 15) and particle size (Barton and Kjærnsli, 1981) respectively. Examples of the stress dependent friction angles obtained from tests on rock fill are given in Fig. 19. Theoretically generated envelopes (Fig. 20) show similar trends.

A more familiar picture of the potential range of shear strength envelopes for tunnel failure in discretely jointed rock masses and in crushed zones is given in Fig. 21. It is assumed that translational failure will be most likely in discretely jointed rock masses, and rotational failure in crushed zones. Rotational failure might also occur in the discretely jointed cases where the excavations are very large compared to the block size.

The peak dilation angles (d_n) indicated on the envelopes at specific stress levels, and tabulated below Fig. 21, are based on the approximate equation:

$$d_n^{\circ} \approx \frac{1}{2} JRC_n \log \left(\frac{JCS_n}{\sigma_n} \right) \dots \dots \dots (10)$$

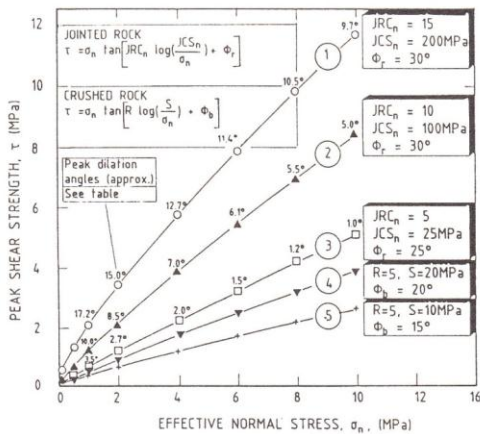
It will be noticed that as the value of (JCS_n/σ_n) approaches 1.0, dilation is suppressed. The five examples of shear strength envelopes given in Fig. 21 illustrate the versatility of equations 8 and 9. The three input

parameters needed to evaluate each equation have physical meaning and can each be measured in principle and usually in practice, by means of Schmidt hammer tests (for JCS and S) and by tilt tests (for JRC, R and ϕ_b) as illustrated in Fig. 22 and 23. In comparison, the parameters needed to extrapolate the Hoek and Brown criterion (m and s in equation 7) for application to rock masses are extremely uncertain, and rely too much on poorly correlated rock mass classification schemes (Q and RMR).

Table 5 summarises some of the assumed characteristics of the five rock masses represented in Fig. 21. Predicted peak friction angles at low, medium and high stress are also given, to aid comparison with the "inter-block shear strength" term; $\tan^{-1}(J_r/J_s)$ given in Table 3.

It should be noted from Table 5 that the predicted peak friction angles obtained from equations 8 and 9 change by exactly JRC degrees or R degrees (i.e. 15°, 10° or 5°) for each order of magnitude change in effective normal stress. This is a fundamental result for rock joints and for rockfill, and will presumably also apply to crushed rock in shear and fault zones, as assumed here.

When stress levels are very high, for example normal effective stresses higher than one half of the value of



Estimates of peak dilation angles (d_n°)

Curve no.	Effective normal stress (MPa)									
	0.1	0.5	1.0	2.0	4.0	6.0	8.0	10.0		
1	24.7	19.5	17.2	15.0	12.7	11.4	10.5	9.7		
2	15.0	11.5	10.0	8.5	7.0	6.1	5.5	5.0		
3	6.0	4.2	3.5	2.7	2.0	1.5	1.2	1.0		
4	5.7	4.0	3.3	2.5	1.7	1.3	1.0	0.7		
5	5.0	3.2	2.5	1.7	1.0	0.6	0.2	0.2		

Values for crushed rock (4+5) are very uncertain

Fig. 21. Estimates of shear strength and dilation angles at peak strength for five examples of jointed and crushed rock.

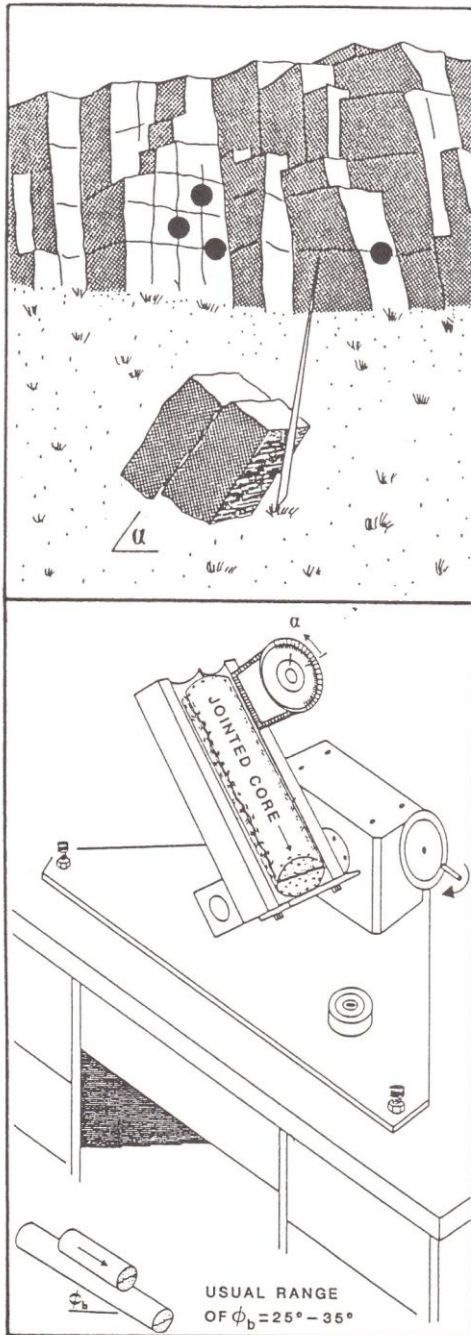


Fig. 22. Tilt tests for obtaining joint roughness (JRC) and basic friction parameters (ϕ_b and ϕ_r) for jointed rock.

JCS, the asperities begin to benefit from confinement and their effective strength rises to $\sigma_1 - \sigma_3$, the confined compression strength. Barton (1976) showed that the peak shear strength is then best described by:

$$\tau = \sigma_n \tan \left[\text{JRC} \log \left(\frac{\sigma_1 - \sigma_3}{\sigma_n} \right) + \phi_r \right] \dots \dots \dots (11)$$

Table 5. Physical descriptions and friction angle ranges for the five rock masses represented in Fig. 21.

Nr.	Physical description of mass	ϕ' at $\sigma_n = 0.1, 1$ and 10 MPa
1	Hard, blocky rock mass, unweathered, rough joints, strongly dilatant	79.5° 64.5° 49.5°
2	Massive, jointed rock mass, unweathered, rough joints, moderately dilatant, wide joint spacing	60.0° 50.0° 40.0°
3	Weak or weathered blocky rock mass, smooth undulating joints, low dilation	37.0° 32.0° 27.0°
4	Weak, crushed, partly clay-bearing zone associated with shear zone, slight dilation	31.5° 26.5° 21.5°
5	Very weak, altered crushed rock and clay, associated with fault zone, non-dilatant	25.5° 20.0° 15.0°

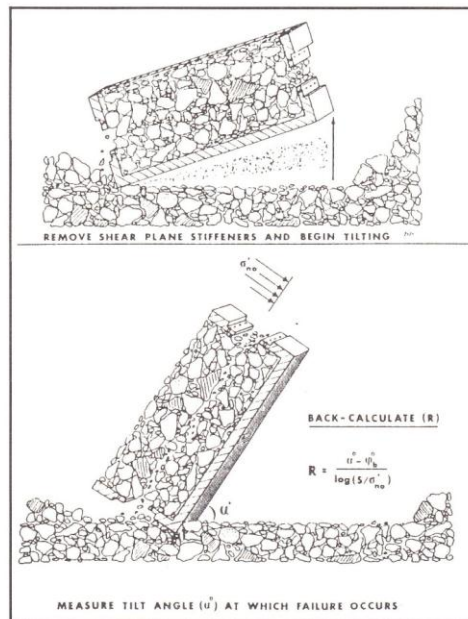


Fig. 23. Method for obtaining an estimate of equivalent particle roughness or interlock (R) for crushed rock, based on a rockfill test method suggested by Barton and Kjærnsli (1981).

Triaxial data needed to derive these values of $(\sigma_1 - \sigma_3)$ will also be scale dependent, but whether the scale corrections for JCS given in Fig. 15 are also relevant to $(\sigma_1 - \sigma_3)$ at high stress is uncertain at present. The corrections for scale will at least be on the conservative side.

(iii) *Stress transformation with dilation*

When analysing the stability of rock masses it is frequently necessary to transform principal biaxial stress components σ_1 and σ_2 into their shear and normal stress components τ and σ_n . These components are assumed to act across specific joint planes inclined at an angle β to the major principal stress. The classical transformation equations given below are based on the assumptions that the medium is isotropic, that the joint planes are imaginary and that they do not slip. At least two of these assumptions are usually violated. In the classical theory

$$\sigma_n = \frac{1}{2}(\sigma_1 + \sigma_2) - \frac{1}{2}(\sigma_1 - \sigma_2) \cos(2\beta) \dots \dots \dots (12)$$

$$\tau = \frac{1}{2}(\sigma_1 - \sigma_2) \sin(2\beta) \dots \dots \dots (13)$$

Besides the violation of assumptions, there is a further very important factor which is not accounted for in equations 12 and 13. As shearing begins along a joint the roughness (if present) is gradually mobilized and results in dilation. This dilation must, by definition, occur out of the plane of the joint. The end result is non-coaxial stress and strain.

It would appear to be simple to correct equations 12 and 13 for this dilation component. However, as indicated in equations 3, 4, 5 and 6 the dilation angle (d_m) mobilized at any instant is a stress and displacement-dependent variable. It also varies with block size owing to the scale effects on both JRC and JCS.

Large scale biaxial shear tests on joints performed by Bakhtar and Barton (1984) indicated that the following versions of equations 12 and 13 provided the best fit to experimental data

$$\sigma_n = \frac{1}{2}(\sigma_1 + \sigma_2) - \frac{1}{2}(\sigma_1 - \sigma_2) \cos[2(\beta + d_m)] \dots \dots (14)$$

$$\tau = \frac{1}{2}(\sigma_1 - \sigma_2) \sin[2(\beta + d_m)] \dots \dots \dots (15)$$

The usual failure to include dilation in stress transformations has important consequences in rock mechanics. It is doubtful that stability analyses currently performed in plane strain environments give enough credit to the potential strength and stress changes caused by slip of non-planar joints. Numerical analyses using joint elements or discrete element codes may also be simulating conservative behaviour in this respect.

It is of interest to note from equations 14 and 15 that the inclusion of a (d_m) component will always increase the normal stress estimate. However, the estimate of shear stress may increase (for $\beta + d_m < 45^\circ$) or de-

crease (for $\beta + d_m > 45^\circ$). When the joint plane is at 45° to the principal stress, the inclusion of the d_m component will therefore cause the normal stress component to increase and the shear stress component to decrease. Both these factors will cause increased difficulty in shearing the rough joints, i.e. they will result in improved stability.

The need to account for dilation both in the estimation of shear strength and in the estimation of the shear and normal stress components emphasizes the extreme influence of this parameter. The difficulty of overcoming dilation in the confined sub-surface environment will tend to limit eventual shearing to very few joints, in place of the mass shearing in the failure of rock masses with plane, non-dilatant or clay-filled discontinuities.

A block shearing out of a tunnel perimeter will usually need to mobilize shear on a minimum of two joint planes simultaneously. This would theoretically result in a maximum dilation of $\varphi(\text{peak}) - \varphi_r$ degrees, i.e. twice the value given by equation 10. This simple result emphasizes the benefit to stability of all joint characteristics that increase the difference between $\varphi(\text{peak})$ and φ_r , i.e. roughness, absence of clay filling, and so forth. It may also be observed that a "reversible-rocking" mode of failure (i.e. slip one on plane at a time and rotation about the other) will result in the least dilation angle and therefore the least build-up of normal stress at any one time.

7. DISCRETE MODELLING OF EXCAVATION BEHAVIOUR

The foregoing treatment of the shear strength and dilation characteristics of jointed rock and crushed rock can be used in principle in continuum analyses, ubiquitous jointed analyses, and distinct element analyses. Simplifications will obviously be needed if only linear joint properties can be handled by the relevant computer code. In such cases, single values of cohesion (c), friction (φ) and where appropriate, shear stiffness (K_s) and dilation (d_n) must be derived for the appropriate stress levels. This in itself may be an improvement over earlier practice, since scale effects will have been incorporated. Continuum models using elastic-plastic formulations will provide some indication of stability problems, but, as stated earlier, may greatly over-estimate the size of the "plastic" zone if dilation is actually occurring in practice, and has not been modelled.

The correct modelling of the dilation accompanying shear in the case of strong rock masses, and of tensile opening of joints, is fundamental to a correct understanding of the way rock masses respond to excavation. Two discontinuum approaches that can be used are physical models and discrete element models. Some illustrations of the capabilities and limitations of these models will be given in this concluding section.

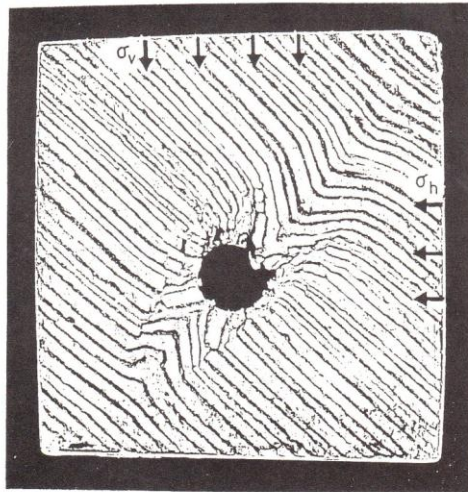


Fig. 24. Example of failure mode visualization using physical models (Bandis, 1987).

(i) *Physical models of regularly jointed rock*

A beautiful illustration of the potential for visualization with physical models is provided by Figure 24. The layered model was developed and tested by Bandis (1987) in current physical model studies of underground openings at NGI. The initial unlined opening was larger than that shown. The very high stress-to-strength ratio applied caused plastic yield, buckling and dilation of the layered media, and resulted in final loading of an instrumented liner. The elliptical zone of "failed material" has a long axis several times the initial opening diameter.

The difficulties of physical modelling increase considerably as one moves from homogeneous models, to layered media, and finally to discretely jointed model rock masses. With these difficulties there also arise limitations. The physical model results illustrated in Fig. 25 show very large displacement. In most cases with such an unfavourable jointing pattern, the walls would have needed heavy rock bolt support before benching down. The reasons for the lack of failure are the very rough model joints (interlocking tension fractures), which have full-scale JRC_n values in the range of 20 to 25, an unrealistic range for almost all rock masses. Nevertheless, a considerable amount can be learned from such models.

Great care was taken to derive realistic input data to represent these model jointed media in FEM continuum analyses (Barton and Hansteen, 1979). Shear tests of the model joints using full-scale block sizes, and normal closure tests on single and multiple joints also using full-scale block sizes, were each used to derive representative moduli for use in the FEM models.

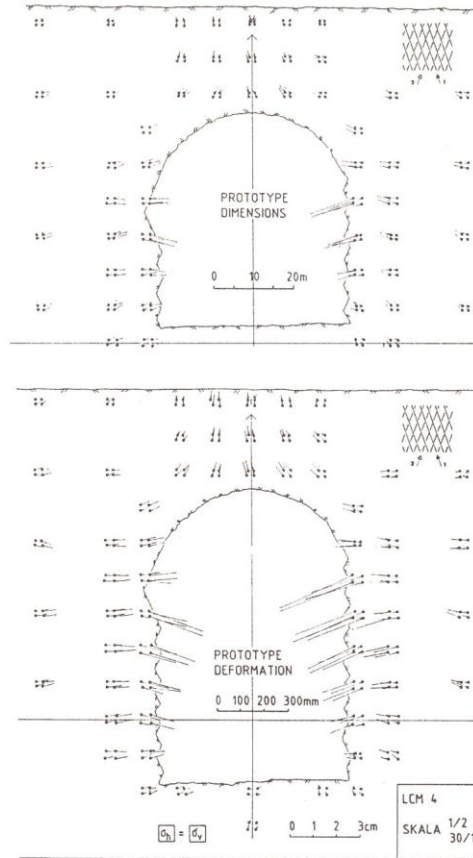


Fig. 25. Deformation in a very large near-surface cavern using a 20,000 block physical model. Note the increasingly non-linear behaviour with increasing wall height.

The results of such a modelling exercise are shown in Fig. 26. The excavation had the same prototype span and isotropic stress as the initial physical model. However the latter was excavated deeper in the two stages shown in Fig. 25. It can be seen that even in the "elastic" portions of the physical model, deformations were roughly an order of magnitude larger than in the finite element model.

One of the reasons for this discrepancy is undoubtedly the hysteresis in unloading illustrated earlier in Fig. 11. However the largest differences are seen in the non-linear shallow wall displacements. The larger displacements seen in the right hand wall are due to the dominance of joint opening over shear displacements. This is because the shear strength of the secondary joint set (2, see inset) is higher than the strength of the pri-

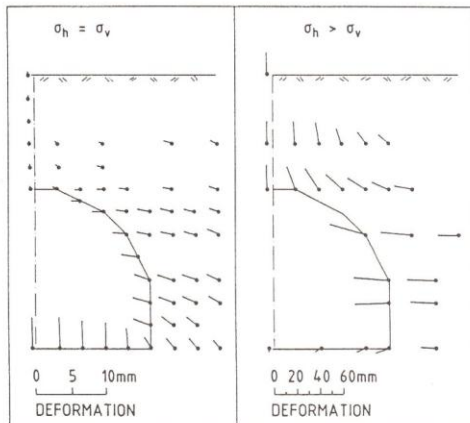


Fig. 26. FEM predictions of behaviour for the near-surface cavern depicted (at later stages of excavation) in Fig. 25.

mary joints which were generated first and were continuous. In this particular model primary joints could open in tension more easily than the secondary joints could shear.

Solutions to the above discrepancies between elastic prediction and non-elastic practice, are available but only "after the event". For example an instrumentation programme would have enabled the designers of such a cavern to "calibrate" their elastic moduli during excavation and obtain a pseudo-fit to the subsequently observed behaviour. Non-linearity (excessive wall deformations) could have been partly avoided in practice with long systematic bolting, if the problem had been anticipated.

The chief reasons for the discrepancy between observed and predicted behaviour in the case cited above are believed to be the hysteresis and volume changes that occurred when stresses were relieved radially, and built up tangentially, by excavation.

A final illustration of the hysteresis seen in physical modelling is shown in Fig. 27. The caverns were excavated in the order 1 to 4 as shown. Each time a new cavern was excavated, the displacement vectors in the newly created pillar remained pointing in the direction of the previous cavern. It almost appeared that pillar deformation was "frozen", presumably due to the very high unloading stiffness (i.e. hysteresis) that we have seen earlier for this type of joint structure (Fig. 11).

(ii) *Distinct element modelling using Cundall's UDEC*

The disadvantages of excessively high joint roughness in tension fracture models (and an unrealistic zero roughness in the case of cast brick models) can be overcome with the advent of distinct element models. The

Cundall (1980) universal distinct element code (UDEC) and the micro computer version (μ DEC) has opened up a new era in rock mechanics design capabilities.

At NGI we are making full use of these capabilities, and have especially concentrated on realistic constitutive modelling of the jointing in these codes. The capabilities of our version of the code (μ DEC-BB) are described by Barton et al. (1987).

Briefly summarized, the BB (Barton-Bandis) joint constitutive model accounts for the non-linearities, scale effects, loading-history effects, shear reversals and deformation-conductivity coupling seen in real rock masses. The non-linear characteristics illustrated in Figs 11 and 13 are incorporated in the model. Full descriptions are given by Barton and Bakhtar (1983).

One particular feature of the BB constitutive model is the ability to calculate the theoretical conducting apertures (e) of the joints. These apertures (typically in the range 10 to 100 μ m) are distinguished from the physical apertures E (typically 50-250 μ m) by an empirical relationship. The physical apertures are a function of normal stress, shear and dilation, and are fundamentally related to the JCS and JRC values for the joint in question. The conductivity (K) of the joints is given by the classic relationship:

$$K = e^2/12 \dots \dots \dots (16)$$

The single example that will be shown here is a numerical model of twin tunnels presently under construction beneath the city of Oslo (Fig. 28). Due to the thick clay deposits in some areas, there is considerable interest in controlling the magnitude of water inflow into the tunnels caused by disturbance of the preinjected zone around the tunnels. Flows larger than about 3 litres/minute/100 metres of tunnel will cause an unacceptable drawn-down of pore pressures in the over-lying clay, resulting in the differential settlements, and building damage.

The geology and joint structure assumed to represent a typical cross-section of the tunnels is shown in Fig. 28 (top). Input data for the joint modelling was obtained by the following means:

1. JRC_0 - from tilt tests on jointed core (Fig. 22)
2. JRC_n - scaling from equation 5
3. JCS_0 - from Schmidt hammer and point load tests
4. JCS_n - scaling from equation 6
5. φ_r - from tilt tests on core sticks (Fig. 22)
6. L_n - natural block size from field mapping
7. e - from borehole pumping tests and use of Snow's statistical method. Note variation with depth.
8. σ_1, σ_2 - from hydraulic fracturing stress measurements and depth - density calculations

Figure 28 (top) illustrates the calculated distribution of conducting apertures (e), which vary from about 60 μ m immediately below the clay, to a minimum of about 20 μ m at 60 metres depth. The two sets of joints (1, 2) in the shale and modular limestone were given slightly

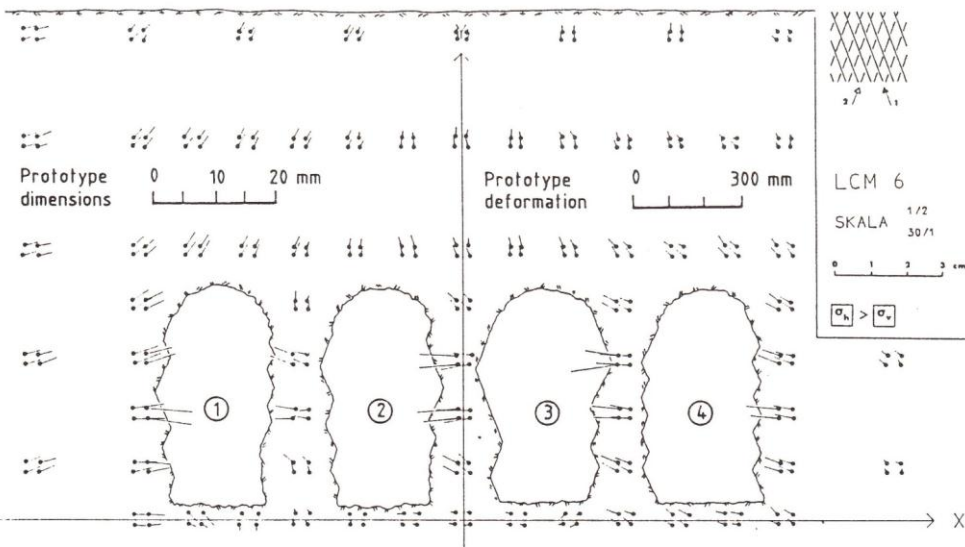
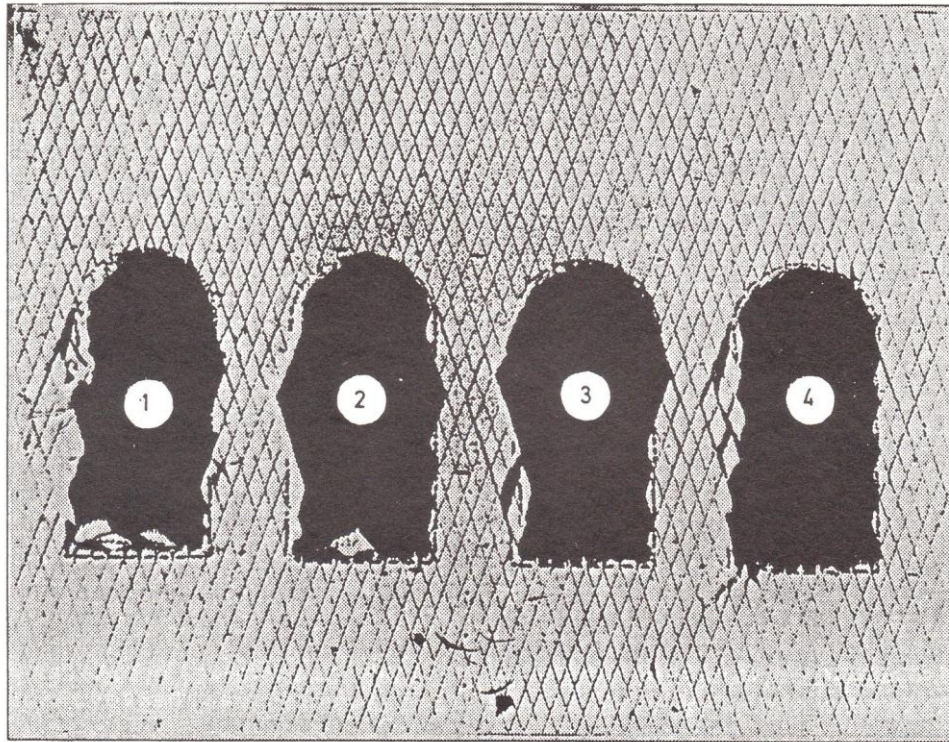


Fig. 27. Upper figure depicts model pillar failures during scaled earthquake loading of unreinforced model storage caverns. Lower diagrams depicts deformation vectors measured following excavation of all four caverns, prior to dynamic loading.

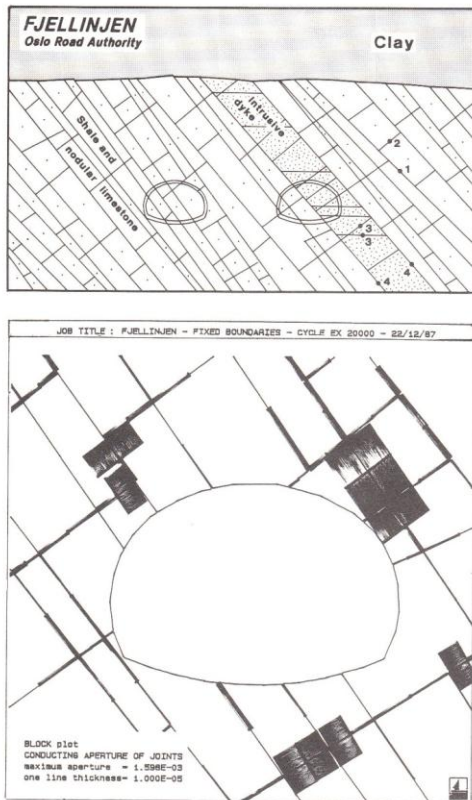


Fig. 28. Application of the distinct element code μ DEC-BB to estimate conducting apertures around twin tunnels excavated in jointed rock (Makurat et al., 1987).

different characteristics, likewise set 3 in the igneous dyke, which was a stronger rock type. The discontinuities bounding each side of the dyke were given fault-type characteristics, i.e. altered (low JCS) and low roughness (low JRC). This resulted in apertures of less than $5 \mu\text{m}$.

The lower diagram in Fig. 28 illustrates in detail the result of excavation on the joint apertures. Note that the liner elements have been given "soft" properties during excavation. Correct concrete stiffness is modelled at a later stage, after rock deformations have fully stabilized, to represent lining operations some distance behind the face. At that stage, full water pressures are built-up in the surrounding rock mass, to investigate final stress levels in the concrete.

The μ DEC-BB model has recently been used for estimating permeability changes in a fractured petroleum reservoir caused by compaction, and for studying deformation in the rock mass surrounding a high pressure gas storage cavern. Its potential uses in rock mechanics are many. However it is important that careful valida-

tion is performed against known cases. A limited number of well controlled in situ tests such as those illustrated in Fig. 11 have been performed, and should be used for careful validation. Physical models of the type illustrated in Figs 25 and 27 also offer an ideal object for validation since the input data has been obtained from "in situ-type" tests, i.e. using the jointed model material itself to conduct shear and deformation tests, as for example illustrated in Fig. 10.

CONCLUSIONS

1. The failure mechanism for excavations in highly stressed intact rocks is believed to be determined by the volume change or dilational characteristics of the failure surfaces themselves. A strong dense rock is unlikely to develop deep intersecting slip surfaces if these surfaces are dilatant at the relevant stress levels. In contrast, a weak porous rock which may compact at the relevant stress levels will readily develop intersecting shear surfaces. For the above reasons, excavations in dense dilatant rock will be more likely to fail by successive development of extension fractures, starting close to the tunnel wall, where dilation is possible. In addition to dilation effects, the more elastic stress state in the case of the strong dense rock will also mean that the stress difference (tangential minus radial) is maximum close to the wall. This is not the case for a compacting porous rock.
2. Underground excavations in jointed or faulted rocks probably fail by translational shear on a limited number of discontinuity surfaces if block sizes are large compared to tunnel dimensions. However, the small block sizes typical of crushed zones may allow rotational shear to occur if the associated dilation is minimal, as in the case of clay-bearing zones. Constitutive models for the strength of rock masses that do not allow for the build-up of stress caused by dilatant failure, will predict larger fracture zones than observed in practice.
3. A constitutive model for the shear strength of rock masses is suggested which is based on a large amount of empirical data. Scale effects caused by block size variations are incorporated in the model, and the strength and dilation can be predicted as a function of shear displacement. Input data for the model can be physically measured using well-tried simple techniques such as tilt tests, roughness profiling, Schmidt hammer and point load tests.
4. Improved predictions of jointed rock mass behaviour around excavations are possible, when discretely jointed rock masses are modelled, either physically or numerically. These show that non-recoverable shear strains, tensile opening of joints, and out-of-plane shear due to dilation are important features.

Numerical distinct element analyses can now be performed that allow one to calculate such features as joint shear, joint aperture, and permeability changes resulting from underground excavation.

ACKNOWLEDGEMENTS

The author would like to thank the following friends, and past and present colleagues for their contributions to this paper, Stavros Bandis, Axel Makurat, Mark Christianson, Harald Hansteen and Khosrow Bakhtar.

Manuel Rocha invited the author to Lisbon in 1972. He requested a contribution to LNEC's workshop on "materials for models, failure of block systems and shear strength". The few days spent at LNEC will be remembered with gratitude. Manuel Rocha's choice of the theme "failure of block systems" was clairvoyant. The present contribution is dedicated to his memory.

9. REFERENCES

- Bandis, S. (1980): *Experimental studies of scale effects on shear strength, and deformation of rock joints*. Ph.D. Thesis, Dept. of Earth Sciences, Univ. of Leeds, England, 385 p.
- Bandis, S. and F. Nadim (1985): *Stability of a deviated wellbore*. NGI contract report.
- Bandis, S. (1987): *Personal communication*.
- Bandis, S., J. Lindman and N. Barton (1987): *Three-dimensional stress state and fracturing around cavities in overstressed weak rock*. Proc. of 6th ISRM Congress, Montreal, Canada, Vol. 2, pp. 769-775.
- Barton, N., R. Lien and J. Lunde (1974): *Engineering classification of rockmasses for the design of tunnel support*. Rock Mechanics, Vol. 6, No. 4, pp. 189-236.
- Barton, N. (1976): *The shear strength of rock and rock joints*. Int. Jour. Rock Mech. Min. Sci. and Geomech. Abstr., Vol. 13, No. 9, pp. 255-279. Also NGI-Publ. 119, 1978.
- Barton, N. and V. Choubey (1977): *The shear strength of rock joints in theory and practice*. Rock Mechanics, Springer, Vienna, No. 1/2, pp. 1-54. Also NGI-Publ. 119, 1978.
- Barton, N. and H. Hansteen (1979): *Very large span openings at shallow depth: Deformation magnitudes from jointed models and F.E. analysis*. Proc. 4th Rapid Excavation and Tunneling Conference. Atlanta, Ch. 77, pp. 1331-1353.
- Barton, N., F. Løset, R. Lien and J. Lunde (1980): *Application of the Q-system in design decisions concerning dimensions and appropriate support for underground installations*. Int. Conf. on Sub-surface Space, Rockstore, Stockholm, Sub-surface Space, Vol. 2, pp. 553-561.
- Barton, N. and B. Kjærnsli (1981): *Shear strength of rockfill*. J. of the Geotech. Eng. Div., Proc. of ASCE, Vol. 107, No. GT7, Proc. Paper 16374, July, pp. 873-891.
- Barton, N. and Bandis, S. (1982): *Effects of Block Size on the Shear Behaviour of Jointed Rock*. Keynote Lecture, 23rd U.S. Symposium on Rock Mechanics, Berkeley, California.
- Barton, N. and Bakhtar, K. (1983): *Rock Joint Description and Modelling for the Hydrothermomechanical Design of Nuclear Waste Repositories*. Terra Tek Engineering TRE 83-10. Submitted to CANMET Mining Research Laboratories, Ottawa, 268 p.
- Bakhtar, K. and Barton, N. (1984): *Large Scale Static and Dynamic Friction Experiments*. Proc. 25th US Rock Mechanics Symp. Northeastern Univ. Illinois.
- Barton, N., A. Makurat, M. Christianson and S. Bandis (1987): *Modelling Rock Mass Conductivity Changes in Disturbed zones*. Proc. 28th U.S. Rock Mech. Symp. Tucson, Arizona, pp. 563-574.
- Cecil, O.S. (1975): *Correlations of rock bolt-shotcrete support and rock quality parameters in Scandinavian tunnels*. Swedish Geotechnical Institute, Proceedings No. 27, Stockholm, 275 p.
- Cundall, P., M. Volgele and C. Fairhurst (1975): *Computerized design of rock slopes using interactive graphics for the input and output of geometrical data*. Proc. 16th U.S. Symp. on Rock Mech., Minnesota (Publ. by ASCE, New York, 1977) pp. 5-14.
- Cundall, P.A. (1980): *A generalized distinct element program for modelling jointed rock*. Report PCAR-1-80, Contract DAJA37-79-C-0548, European Research Office, US Army. Peter Cundall Associates.
- Hoek, E. and E.T. Brown (1980): *Underground excavations in rock*. Institution of Mining and Metallurgy, 527 p.
- ISRM (1978): *Suggested methods for the quantitative description of discontinuities in rock masses*. (Coordinator, N. Barton), Int. J. Rock Mech. Sci. and Geomech. Abstr., Vol. 15, pp. 319-368, Pergamon.
- Leps, T.M.: *Review of shearing strength of rockfill*. Journal of the Soil Mechanics and Foundation Division, ASCE, Vol. 96, No. SM4, Proc. Paper 7394, July 1970, p. 1159-1170.
- Makurat, A., N. Barton, M. Christianson, P. Chryssanthakis and G. Vik (1987): *Fjellinjen tunnel behaviour predictions using distinct element computer modelling*. NGI contract report (In Norwegian).
- Maury, V. (1987): *Observations, researches and recent results about failure mechanisms around single galleries*. ISRM commission report, Proc. of 6th ISRM Congress, Montreal, Vol. 2, pp. 1119-1128.
- Ortlepp, W.D. and N.C. Gay (1984): *Performance of an experimental tunnel subjected to stresses ranging from 50 MPa to 230 MPa*. Proc. of ISRM Symp. "Design and Performance of Underground Excavations", Publ. British Geotechnical Society, London. pp. 337-346.
- Wagner, H. (1987): *Design and support of underground excavations in highly stressed rock*. Keynote paper, Proc. of 6th ISRM Congress, Montreal (Vol. 3, reprint by courtesy of author).